Microscale characterization of prostate biopsies tissues using optical coherence elastography and second harmonic generation imaging

Ling Yuting[1,2,5], Chunhui Li[1,2,5], Kanheng Zhou[1,2], Guangying Guan[1,2], Paul L Appleton[3], Stephen Lang[4], David McGloin[2], Zhihong Huang[1,2] and Ghulam Nabi[1]

Photonics, especially optical coherence elastography (OCE) and second harmonic generation (SHG) imaging are novel high-resolution imaging modalities for characterization of biological tissues. Following our preliminary experience, we hypothesized that OCE and SHG imaging would delineate the microstructure of prostate tissue and aid in distinguishing cancer from the normal benign prostatic tissue. Furthermore, these approaches may assist in characterization of the grade of cancer, as well. In this study, we confirmed a high diagnostic accuracy of OCE and SHG imaging in the detection and characterization of prostate cancer for a large set of biopsy tissues obtained from men suspected to have prostate cancer using transrectal ultrasound (TRUS). The two techniques and methods described here are complementary, one depicts the stiffness of tissues and the other illustrates the orientation of collagen structure around the cancerous lesions. The results showed that stiffness of cancer tissue was ~ 57.63% higher than that of benign tissue (Young's modulus of 698.43 ± 125.29 kPa for cancerous tissue vs 443.07 ± 88.95 kPa for benign tissue with OCE. Using histology as a reference standard and 600 kPa as a cut-off threshold, the data analysis showed sensitivity and specificity of 89.6 and 99.8%, respectively. Corresponding positive and negative predictive values were 99.5 and 94.6%, respectively. There was a significant difference noticed in terms of Young's modulus for different Gleason scores estimated by OCE (P-value < 0.05). For SHG, distinct patterns of collagen distribution were seen for different Gleason grade disease with computed quantification employing a ratio of anisotropic to isotropic (A:I ratio) and this correlated with disease aggressiveness.

Prostate cancer (PCa) is a heterogeneous disease with a multifocal origin.[1] The diagnosis is confirmed by histopathology of tissue samples obtained through transrectal ultrasound (TRUS)-guided biopsies. The disease is screened/suspected by a high serum prostate-specific antigen (PSA) levels and/or abnormal digital rectal examination (DRE). Cancer is characterized following histopathological verification under a microscope using the Gleason scoring system[2] by a pathologist. The information obtained is utilized according to a risk-stratified approach and the treatment options are discussed with patients. However, the data obtained from the histopathological examination of the radical prostatectomy specimens indicate that a large disparity existed between the Gleason score of biopsy samples and the radical prostatectomy specimen. This incongruity has implications for patient counseling and therapy. In a meta-analysis of 14 839 patients, Cohen et al[3] demonstrated that only 58% of patients' biopsy Gleason grade accurately predicted the final Gleason grade of radical prostatectomy. Similarly, Serefoglu et al[4] provided evidence that just 43.3% of patients had the same Gleason score for preoperative biopsy and postoperative radical prostatectomy specimens with the false-negative rate of more than 30%. Thus, the healthcare challenge is to improve accuracy of the Gleason grade characterization of initial prostate biopsies as this would allow for more appropriate therapeutic choices.

Radical prostatectomy, a surgical option for localized disease seeking to cure, is primarily meant to remove all malignant tissues while preserving neurovascular bundles and

[1]Division of Cancer Research, Ninewells Hospital and Medical School, University of Dundee, Dundee, UK; [2]School of Science and Engineering, University of Dundee, Dundee, UK; [3]Dundee Imaging Facility, Ninewells Hospital and Medical School, University of Dundee, Dundee, UK and [4]Department of Pathology, Ninewells Hospital and Medical School, University of Dundee, Dundee, UK
Correspondence: Professor G Nabi, MCh, MD, FRCS (Urol), Division of Cancer Research, Ninewells Hospital and Medical School, University of Dundee, Dundee DD1 9SY, UK.
E-mail: GNabi@dundee.ac.uk
[5]These authors contributed equally to this work.

continence mechanism for robust quality outcomes.[5] Intraoperatively, the decision is based on a combination of preoperative imaging, biopsy histology, and macroscopic assessment. The final decision on margin status, however, is confirmed after many days of surgery, which is least helpful as corrective surgery is impossible in contrast to breast cancer.[6] Patients with positive surgical margins have a higher risk of cancer recurrence and necessitate further treatment. An intraoperative diagnostic technique that can reliably assess the margin status of tissues with regards to presence or absence of cancer cells would have a huge potential implication for surgical techniques and PCa patient outcomes. Frozen sectioning and imprint cytology are currently used but often unreliable.[7,8] Optical imaging techniques have been explored to address this issue in a number of previous publications. A number of optical imaging techniques have been proposed, including optical coherence tomography (OCT)[9] and Raman spectroscopy,[10] however the utility of tissue stiffness measurements has not been reported.

The stiffness difference perceived via DRE has been an effective technique for centuries to suspect PCa. Tissue from PCa has a higher elastic modulus than the normal prostate glandular tissue.[11] Changes in elasticity may indicate an abnormal pathologic process as the elasticity of tissue is a result of increased cell density and collagen deposition.[12,13] Measuring the elastic properties of prostate tissue has received increasing attention recently.[14–17] This can be deduced using ultrasound-based technology.[18] However, other imaging modalities such as magnetic resonance imaging (MRI) and OCT are also reported. Optical imaging with the advantage of a much higher microscale resolution has the potential to enhance the application limit of ultrasound and MRI.[19] Furthermore, this technology may uncover the microscopic heterogeneity of prostate tissue and even early tumors.

The working principle of OCT is similar to ultrasound, but it uses light instead of sound waves. OCT is a real-time, *in vivo* and non-invasive optical imaging technology with a high resolution and a fast acquisition speed. The use of OCT to perform elastography is a technique known as optical coherence elastography (OCE) with sub-nanometer displacement sensitivity.[20] Although the penetration depth of OCE (1–2 mm) is much less than that of ultrasound and MRI, this limit can be overcome by developing fiber-optic like needle probes for elastography measurements.[21,22] Our preliminary work utilizing a novel quantitative OCE method clearly presented the promising results in *ex vivo* PCa detection with 120 biopsies from 10 patients.[17] We demonstrated that OCE can reliably differentiate between benign and malignant prostate tissues with a high diagnostic accuracy. The method also has potential for characterizing different grades of PCa based on the change of tissue morphology and quantitative mechanical properties.

The preliminary study using OCE was limited to 10 patients, and the impact of Gleason score on stiffness needed further confirmation. Also, it is currently poorly understood whether the resulting elasticity images are faithful representations of the underlying microscale elastic properties. Extracellular matrix (ECM) remodeling[23] is significant in cancer progression with collagen as the dominant structural component providing mechanical strength and flexibility to tissue. A technique that can identify and characterize features of the epithelial–stromal microenvironment is of great diagnostic potential and interest. An extension of our preliminary work was required along with peri-tumor collagen characterization using second harmonic generation (SHG) imaging.

SHG microscopy is a popular imaging tool for visualization and characterization of non-centrosymmetric 3D structures such as collagen in medicine and biology.[24] Fourier transform second harmonic generation (FT-SHG)[25–27] was applied to quantify the changes in collagen morphology. The initial results[28] indicated that the collagen in the prostate stroma had different patterns in normal and malignant biopsies depicted by SHG images, and the fibers of the malignant tissue tended to have a higher degree of preferred orientation than that which were normal as quantified by FT-SHG. The A:I ratio parameter based on the ratio between anisotropically and isotropically aligned collagen fibers, was applied to compute the regularity in collagen fiber orientation and correlate it with a variety of Gleason scores. On the basis of the initial results, we proceeded to test these results in a larger sample size.

We hypothesized that a combination of OCE and SHG imaging would narrow down the Gleason grade discrepancy between prostate biopsies and radical prostatectomy specimen. The study had the following objectives:

(1) To estimate the diagnostic accuracy of OCE (2D and 3D) and SHG in the detection and grade characterization of PCa in *ex vivo* prostate biopsies.
(2) To determine the reliability of both these techniques in predicting the final radical prostatectomy Gleason grade of the disease from measurements of Young's modulus established through OCE and orientation of collagen according to SHG.

PATIENTS AND IMAGING METHODS
Selection of Cohort
This was a prospective study with institutional ethics approval (14/ES/0049) and informed consent from patients to report the research data. Seventy patients were recruited into the study, including 10 cases reported previously in our feasibility study. With a slight modification of the protocol from the feasibility study, we recruited 60 patients (age range 56–85) undergoing TRUS-guided biopsies for suspected PCa between April 2014 and December 2015. Thirty-seven men were confirmed to have PCa with a Gleason score ranging from 6 to 9. Amongst those without cancer, a number of histological findings were reported, such as benign prostatic hyperplasia

(BPH), atypical small acinar proliferation (ASAP), and prostatitis, and/or prostatic intraepithelial neoplasia (PIN).

We tested our hypothesis that *ex vivo* measurements of tissue stiffness on biopsy material may have an improved prediction of the final Gleason grade of radical prostatectomy in a small group of 11 patients undergoing laparoscopic radical prostatectomy employing a rapid prototyping mold-based approach published previously.[29]

TRUS-Guided Biopsies

All participants underwent the standard 12-core TRUS-guided biopsies of prostate gland using an 18-G needle. The size of the biopsy samples ranged from ~0.8 to 1.2 mm in diameter and 5 to 20 mm in length. Biopsies were immediately fixed using 10% neutral buffered formalin (50 ml) and stored in separate containers. The samples were allowed to be fully fixated over 24 h according to the previous study protocol.[30] Measurement of stiffness point-wise along the length of biopsy specimen was conducted according to the OCE technique. The specimens were then analyzed by an experienced uro-pathologist (SL) with a routine histological protocol via hematoxylin and eosin (H&E) staining. The uro-pathologist was unaware of stiffness data. The detailed pathological report included the presence/absence of malignancy, grade of cancer, percentage of cancer involvement in each core, and perineural infiltration.

The histopathological data of a total of 720 cores were categorized into non-cancerous prostate tissue (448 core biopsies) and cancerous prostate tissue (272 core biopsies), of which one patient was diagnosed with carcinosarcoma. The PCa tissue was further categorized into seven sub-groups based on different Gleason scores: 3+3, 3+4, 3+5, 4+3, 4+4, 4+5, and 5+4 in 58, 54, 4, 46, 48, 39, and 11 core biopsies, respectively. For estimation of collagen orientation around cancerous lesions using SHG microscopy, 42 biopsy samples were imaged (36 cancerous and 6 benign). The cancerous group was further divided into six sub-groups based on different Gleason scores: 3+3, 3+4, 4+3, 4+4, 4+5, and 5+4 with six core biopsies in each group.

Optical Coherence Elastography

The system setup of OCT/OCE was based on our previous report[17] with slight modification. Briefly, the OCE consists of two main parts: vibration stimulation and displacement detection. An electromagnetic actuator was used for vibration stimulation, driven by a sine-wave-modulated signal with the modulation frequency of ~8 kHz. The maximum actuator displacement applied to the specimens was ~1 μm to ensure the strain generated was in a pure linear-elastic regime. The vibrations could be transmitted from the actuator to compress the specimens and trigger vibration in the axial direction. Detection of the vibration signal was performed via phase-sensitive optical coherence tomography (PhS-OCT) system. It employed a superluminescent diode (SLD) as the light source, with a central wavelength of ~1302 nm and

bandwidth of ~85 nm, implemented by a spectral domain configuration. The sample arm had an objective lens of ~18 mm focal length to deliver the detection light onto the specimens and coupled the vibration signals into the PhS-OCT for detection. The system had an axial resolution of ~8.8 μm and a transverse resolution of ~7.9 μm in air. The acquisition rate was determined by the spectrometer employed in the system which had a maximum rate of ~76 000 A-scans/s. The dynamic range of the PhS-OCT system was measured to be ~100 dB at 0.5-mm axial depth with a phase noise of 3 mrad. However, the SNR in the region of interest (ROI) of the tissue sample was ~50 dB.

For the acquisition of a cross-sectional 2D structure and elastogram, the OCE probe beam stayed for 512 repeats during the A-line scan at every spatial location sequentially within the B-scan (a total of 256 locations) mode, whereas the actuator repeatedly fired the stimulus. Thus, a complete B-scan consists of 512×256 A-scans. The specimens were then scanned cross-sectionally from one end to the other at an interval of 50 μm. This ensured adequate details obtained to generate a 3D structure and elastogram of each biopsy. Further, the system had a minimized acquisition time that enabled that each pair of structure and elastogram were recorded from the same region of tissue. The acquisition time for a 3D OCE data set was 3 min for images with dimensions (*xyz*) of 3 mm×2 mm×2 mm.

After the acquisition of one data set, the transitional stage was moved 2.5 mm in the *y* direction for the next acquisition, and this was repeated until the whole biopsy core was scanned. During the OCE scanning, the biopsy core was placed on a 2% agar phantom with a thickness of ~8 mm, which was an elasticity reference.[31] The total scanning time for each biopsy was dependent on the biopsy length. The raw structure and elastogram data sets were processed by MATLAB R2015b (The MathWorks, Natick, MA, USA) for data processing[32] to generate structure and elastogram frames for each B-scan. The frames were then imported into Amira (Mercury Computer Systems, Berlin, Germany) and reconstructed into 3D data sets at full resolution.

Multiphoton SHG Microscopy

Images for the SHG technique were acquired with an upright multiphoton microscope TCS SP8 MP (Leica) at the Dundee Imaging Facility. The tunable near-IR laser (Spectra-Physics InSight DeepSee) produced linearly polarized pulses spectrally centered at 880 nm. After spatial filtering and collimation, the beam was sent to the galvo-scanner. Incident light at 880 nm was focused onto the sample with a Leica HC PL Fluotar ×10 0.3NA objective. Owing to the momentum conservation, the SHG signal was especially directional and emitted mainly in the forward direction, being collected by a 0.9 NA condenser lens. The SHG signal was then filtered through a laser blocking filter (SP 680) and an SHG bandpass filter (440/20) and subsequently being detected with a standard photo-multiplier. The SHG laser power was adjusted to around
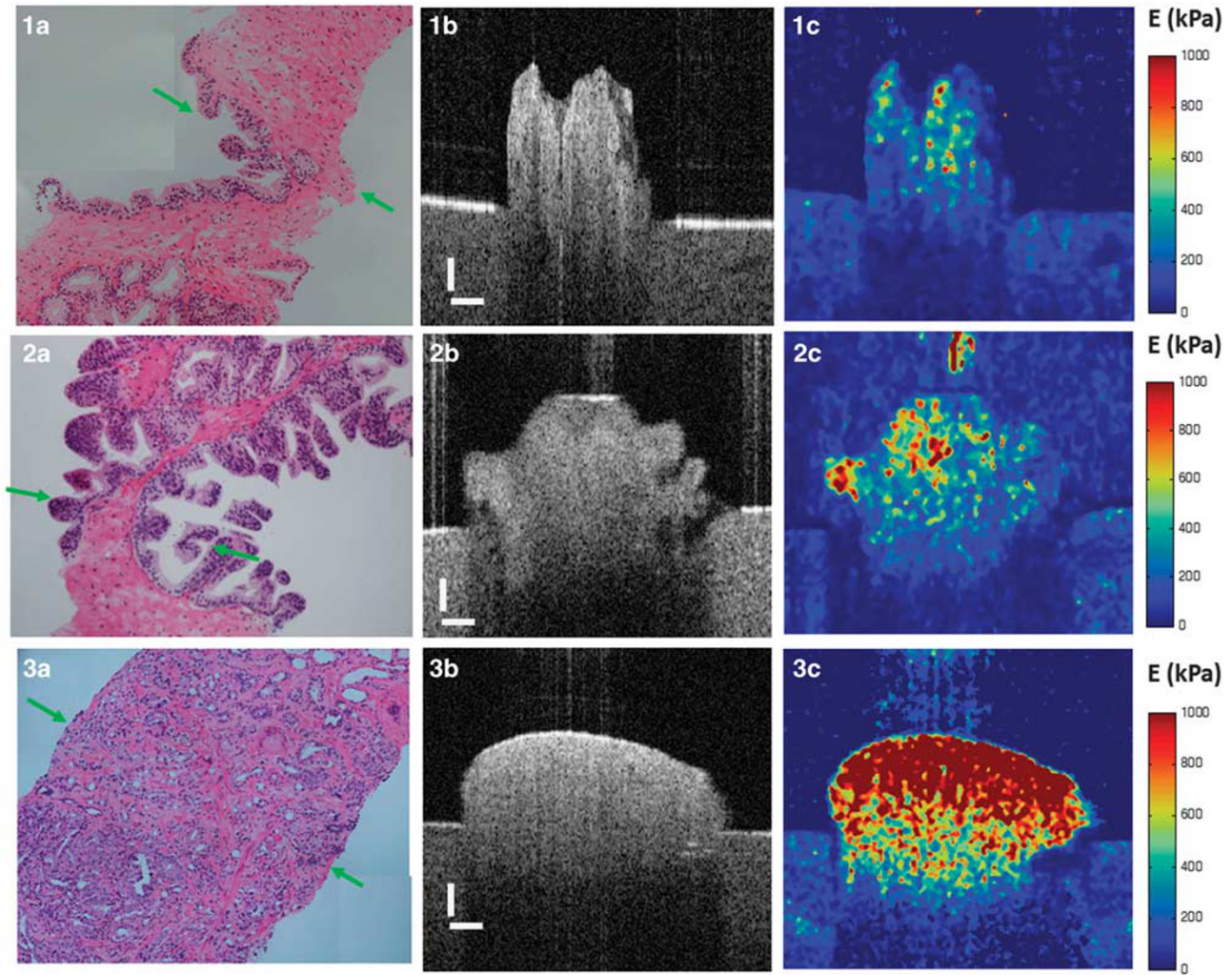
Figure 1 Images of (**a**) histology, (**b**) cross-sectional OCT structure, and the corresponding (**c**) OCE elastogram of (1) benign prostate tissue, (2) prostatic intraepithelial neoplasia (PIN) and (3) malignant PCa with Gleason score 4+3. The scale is 200 μm. Young's modulus is in the unit of kPa.

50 mW so that sufficient signals were obtained without any obvious damage to the sample. The transmitted light image was obtained from a 488 nm laser and collected in the forward transmitted light position via a 483/32 filter. A combination of z-stack and tile scan was utilized to acquire the whole area of the biopsy section automatically. Through identical settings, 12-bit images of 3352×3352 pixels were obtained using LAS X (Leica Application Suite X).

The alignment of collagen fibers in each section was quantified by FT-SHG as described in the previous report.[28] The processing algorithms were developed in Matlab R2015b (The MathWorks, Natick, MA, USA). This method was employed to identify the quantitative parameters that represent collagen orientation in the prostate biopsies through assessment of the spatial frequencies within an image using a 2D-FT. In a given plane, the direction the majority of fibers tend to align along is defined as the preferred orientation. Through 2D-FT, the high amplitudes

on average oriented perpendicularly to the preferred orientation. To calculate the preferred orientation more rapidly, the original image was firstly divided into sub-images and categorized into three groups: negligible, anisotropic, or/and isotropic. Negligible was defined if the SHG signal intensity in the area was low or nearly dark. The sub-images where collagen fibers had preferential orientation were labeled as anisotropic and the sub-images with many different directions were labeled as isotropic. Lastly, the overall orientation of the collagen fibers in each entire biopsy was quantified by applying the A:I ratio (the ratio of the number of anisotropic to isotropic sub-images).

Statistical Methods

A systematic statistical method was conducted by a statistician blinded to the OCE/SHG and histological data to investigate the reliability of quantitative OCE in differentiating benign and malignant prostate tissues as well as determining the

sensitivity and specificity of this technique. Young's modulus (kPa) estimated from 720 biopsy cores by the OCE system was compared amongst malignant and benign tissues, as well as different Gleason scores. All the analyses were performed with SPSS v.22 (SPSS, Chicago, IL, USA). Differences between the groups were evaluated according to the Games–Howell test. A *P*-value of 0.05 was considered to be statistically significant.

RESULTS
### 2D Structural and Elastography of Prostate Biopsies

The images obtained from OCT and OCE imaging were directly compared with the images acquired after standard histopathological processing. The results suggested that micro-architecture on the order of $10 \mu m$ can be distinguished in prostatic tissue. Figure 1 presents the histological photo, OCT structural image, and OCE elastogram of various catalogs of prostate tissue. A clear biopsy–agar–air boundary can be seen in both the structural and elasticity images. The signal strength of the elastogram decreased with the rise in imaging depth. This is because the accuracy of the phase measurement for the elastogram relies on the intensity level of the structural image, and the intensity of the vibration signals reduced at deeper locations.

The top of Figure 1 presents the images of histology, structure and elastogram of benign prostatic tissue. In the histological image Figure 1(1a) shows, an irregular boundary and/or hollow structure indicates the benign glandular lumens. However, there is no difference seen between the glandular lumens and the surrounding stromal tissue. For example, smooth muscle and fibroblastic stroma cannot be distinguished. Figure 1(1c) demonstrates in detail the elastic variance in various kinds of tissue in detail. The elasticity of the glandular lumens is higher than that of the stromal tissue. By comparing all elastograms and histological photos of benign prostate tissue, it is found that the smooth muscle has the lowest stiffness at 378.4 kPa (s.d. = 48.9 kPa). The glandular lumens have higher stiffness at 530.6 kPa (s. d. = 30.9 kPa), whereas the stiffness of the fibroblastic stroma varies at 518.4 kPa (s.d. = 82.5 kPa).

Images of the histology, structure, and elastogram of the PIN are illustrated in the middle of Figure 1. Subtle differences in tissue structure amongst benign, BPH, ASAP, and PIN tissues can be elucidated in the structural images. The glandular lumens in Figure 1(2b) has a more irregular surface, which is confirmed by the histological phenotype in Figure 1(2a). The difference between PIN and benign prostate tissue is more evident in the elastogram Figure 1(2c). The PIN has higher stiffness than benign prostate biopsies, whereas BPH and ASAP have lower stiffness than benign prostate tissue. Notwithstanding, significant overlaps still existed amongst the elasticity range of the aforementioned kinds of prostate tissues.

A typical malignant glandular tissue with a Gleason score of 4+4 is found at the bottom of Figure 1. The lumens here serve as the main characteristic histologically to determine PCa aggressiveness. In Figure 1(3a), the malignant structures are significantly smaller than those in the benign glandular tissue
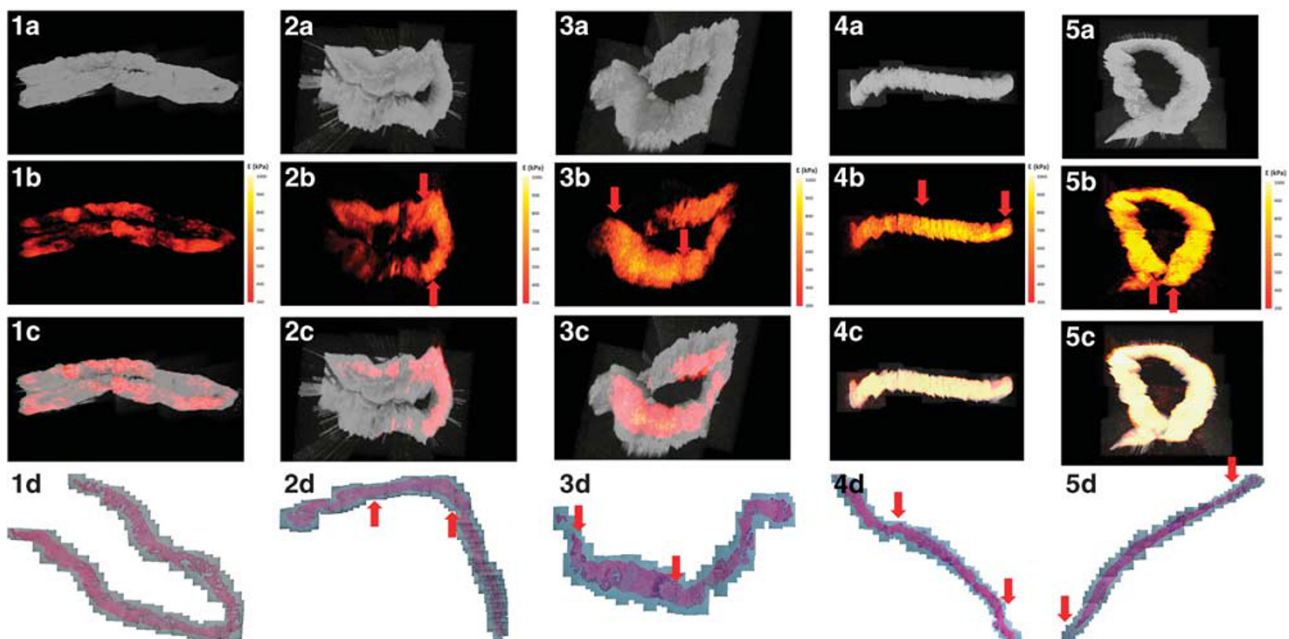
Figure 2 3D visualization of (1) benign and PCa biopsies with Gleason score (2) 3+3 with cancer involvement 30%, (3) 3+4 with cancer involvement 40%, (4) 4+4 with cancer involvement 60%, and (5) 4+5 with cancer involvement 80%. (**a**) OCT structural image, (**b**) OCE elastograms, (**c**) overlaid images from en-face views, and corresponding (**d**) histological photos. The red arrows in **b** and **d** indicate the origin and end of malignancy.

and range in size from 10 to 50 μm. Therefore, OCT can identify micro-architecture of 10 μm or greater. Cancerous prostate tissue is observed to have a well-rounded shape without irregular gland lumens with higher light reflectivity. A significant increase of tissue stiffness is observed in Figure 1 (3c). Therein, it is also noticed that the stiffer the prostate biopsy, the higher the Gleason sum, and the more aggressive the PCa.

3D Structural and Elastography of Prostate Biopsies

Figure 2 delineates 3D images of the structure and elastogram from benign and different grades of malignant PCa prostate biopsies. The en-face views of four different forms of data (structure, elastogram, overlay, and histology) were obtained from five prostate cores of benign and different grades of malignant PCa with a Gleason sum 6 to 9. In Figure 2b, an ascending trend of elasticity signal is observed in the region of malignant PCa with the concomitant increase in the Gleason sum. In addition, the area of malignancy can be better portrayed by elastograms from OCE imaging than with a histological photograph. The bright areas in Figure 2b match the areas labeled by the red arrows in Figure 2d indicating the origin and end of the malignant area in the prostate biopsies.

Diagnostic Accuracy of OCE

In this study, three methods were utilized for statistical analysis in comparing different biopsy cores: (1) the average Young's modulus method, which is the weighted average Young's modulus value over the whole area associated with each biopsy, (2) the maximum Young's modulus which is the maximum Young's modulus value of all the B-scan elastograms across all biopsies, and (3) the threshold method which is the percentage of the data points comprising the Young's modulus values higher than 600 kPa among the data set for each biopsy.

The results from the statistical analysis of PCa and benign prostate tissue are illustrated and compared with the whisker plots in Figure 3. From these plots, a significant increase in stiffness can be observed (P-value < 0.001) between the benign prostate tissue and PCa using any of the aforementioned three methods. In Figure 3a, by comparing the elasticity data obtained from OCE and the corresponding histological report, PCa was suspected with Young's modulus higher than 600 kPa. Figures 3b and c demonstrate that a certain stiff area exists in the non-PCa biopsies, but most of it is below 30% which could suggest very low cancer involvement, but not recognizable.

The plot of the ROC analysis in Figure 4 is intended to evaluate the ability of quantitative OCE to diagnose PCa with the aforementioned three statistical analysis methods. Over 90% of the area is under the ROC curve. Among the three curves, the method of using average Young's modulus has the highest area under the curve (AUC; 93.9%), which supports OCE as a promising with a high capability for the diagnosis of PCa. The threshold method has an AUC of 93.6%, and the maximum method has the lowest AUC, albeit a still high accuracy (91.6%). On the basis of the threshold method for diagnostic accuracy, the biopsies with a Young's modulus higher than 600 kPa were treated as positive results for PCa, and the others were negative and can be considered cancer-free (benign) biopsies. Compared to the histological results, the data analysis showed that the sensitivity and specificity of the threshold method was 89.6 and 99.8%, respectively. Moreover, the positive and negative predictive values calculated for this technique were 99.5 and 94.6%, respectively.

The relationship between the Gleason score and the estimated Young's modulus is compared in Figure 5. The presence of the Gleason score in the histopathological results is of clinical significance when making an optimal decision for the individual patient. The average method stands out from the other methods. A significant difference was noticed amongst Young's modulus of different Gleason scores estimated by OCE (P-value < 0.05) except for Gleason score 7 and 8 (P-value = 0.765).

Collagen Orientation

According to the previous pilot study, a predominant reticular pattern of collagen fibers was seen in cancerous lesions in contrast to the more common papillary pattern of the benign
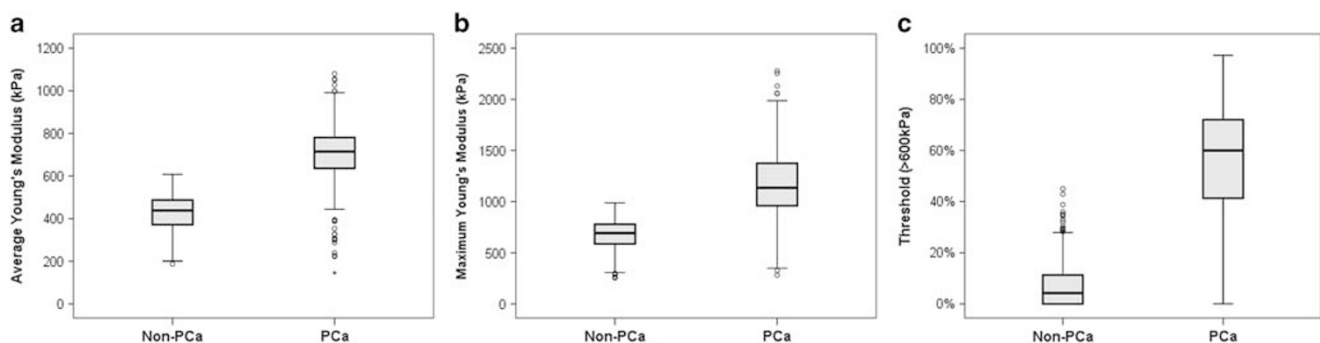
Figure 3 Whisker plots of correlation of Young's modulus (kPa) and pathological outcomes using (**a**) average method, (**b**) maximum method, and (**c**) threshold method.
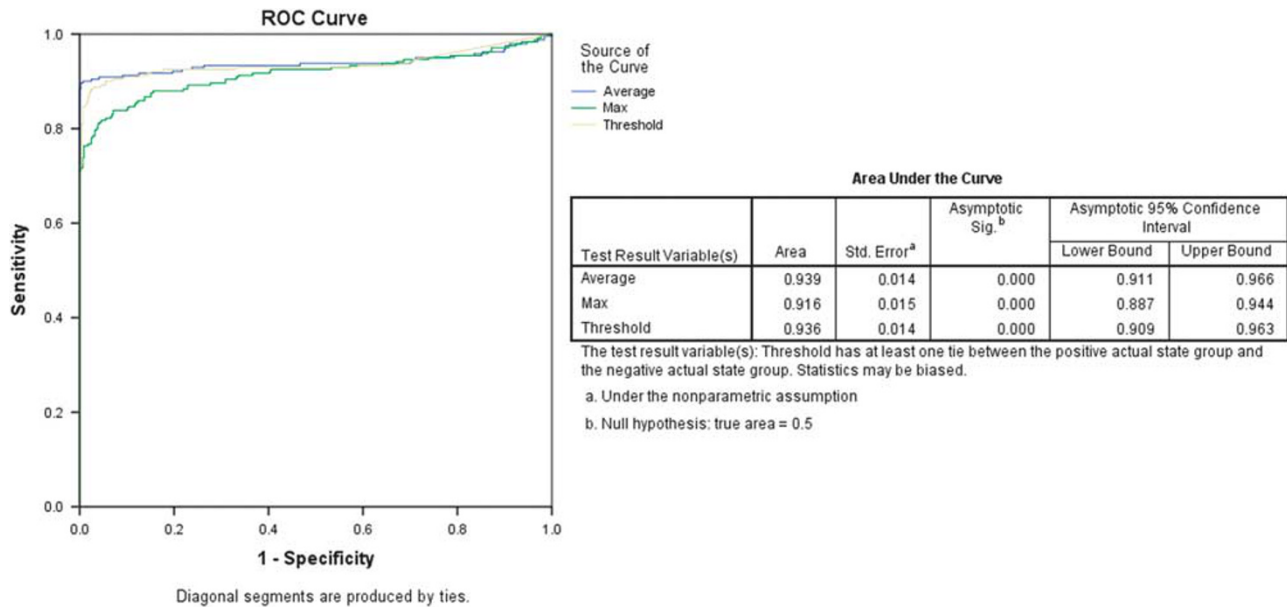
Figure 4 ROC curves of PCa *vs* benign using three statistical analysis methods.
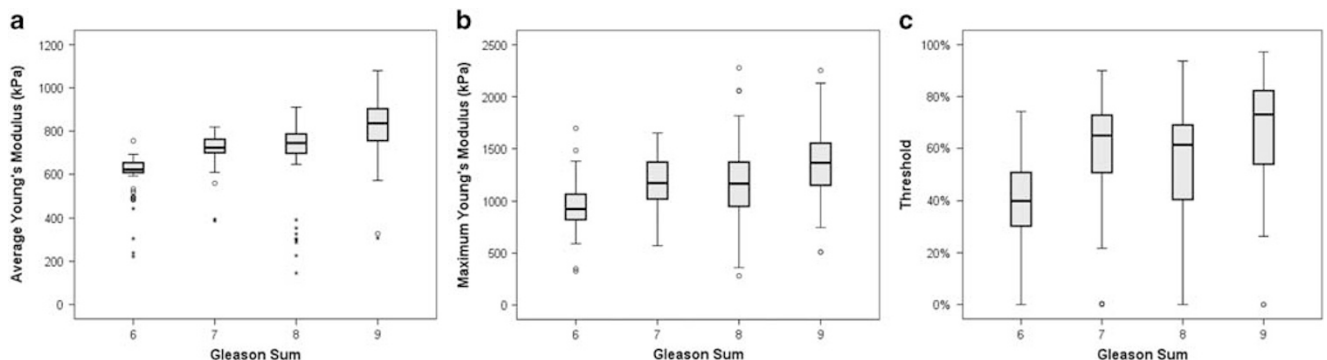

Figure 5 Whisker plots of correlation of Gleason scores and Young's modulus (kPa) using (**a**) average method, (**b**) maximum method, and (**c**) threshold method.

part of tissues. However, the reticular pattern disappeared in highly-aggressive cancer such as Gleason 4+5. The A:I ratio was applied to compute the regularity in collagen fiber orientation and utilized to compare Gleason scores across prostate biopsies. Generally, malignant cores were found to be more aligned than those that were normal. Moreover; the A:I ratio increased with a higher Gleason score, which meaning that the collagen fibers tended to be more oriented as the prostate cancer became more aggressive.

It was noted and discussed in the previous study that a small fluctuation occurred with an advanced grade of cancer and that a Gleason score of 4+3 had a lower A:I ratio than a Gleason score of 3+4. The new study with an increased number of slides (42 in total) had similar findings. As shown in the Whisker plot in Figure 6a, the orientation of the collagen fibers demonstrated a rising trend when the cancer was more aggressive, but it decreased for higher grade of

malignancy, such as Gleason 8 and 9. Figure 6b illustrates that a Gleason 4+3 is less anisotropic than Gleason 3+4, which is consistent with what was observed in the previous study. Moreover, a Gleason score of 4+5 also had a higher tendency of alignment than a Gleason score of 5+4 in Figure 6c. Therefore, a higher primary grade led to less oriented collagen fibers and a lower A:I ratio for a scenario of the same Gleason sum.

Collagen Orientation and Tissue Stiffness
Elastography can detect subtle elasticity differences across the biopsy with a high-resolution OCT system, and SHG imaging can illustrate collagen distribution and orientation with multiphoton microscopy. The correlation between OCE and SHG imaging is key to the understanding of the increased stiffness in malignant tissue. It was noted that the lower the Young's modulus, the less oriented the collagen fibers will be.
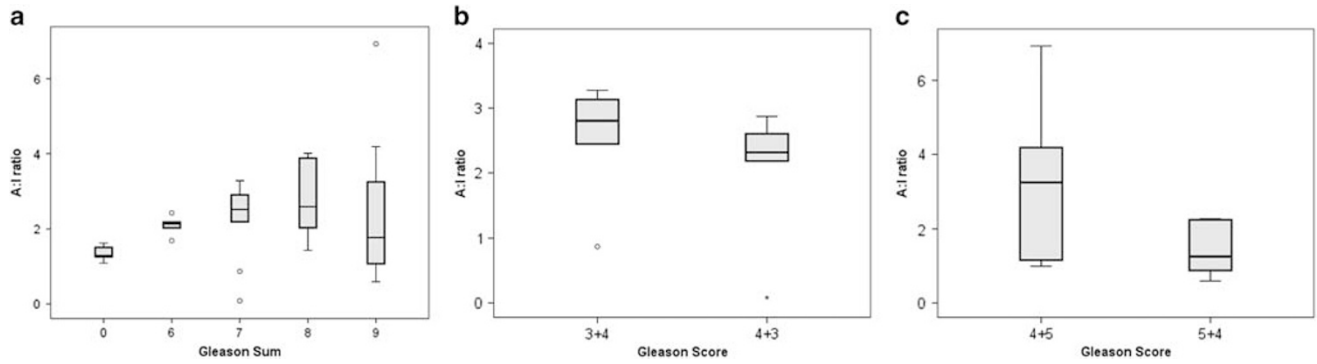
Figure 6 Whisker plots of the relationship between collagen orientation (A:I ratio) and different Gleason scores. (**a**) Comparison among benign and malignant biopsies with different Gleason scores from 6 to 9, (**b**) comparison between Gleason 3+4 and 4+3, and (**c**) comparison between Gleason 4+5 and 5+4.
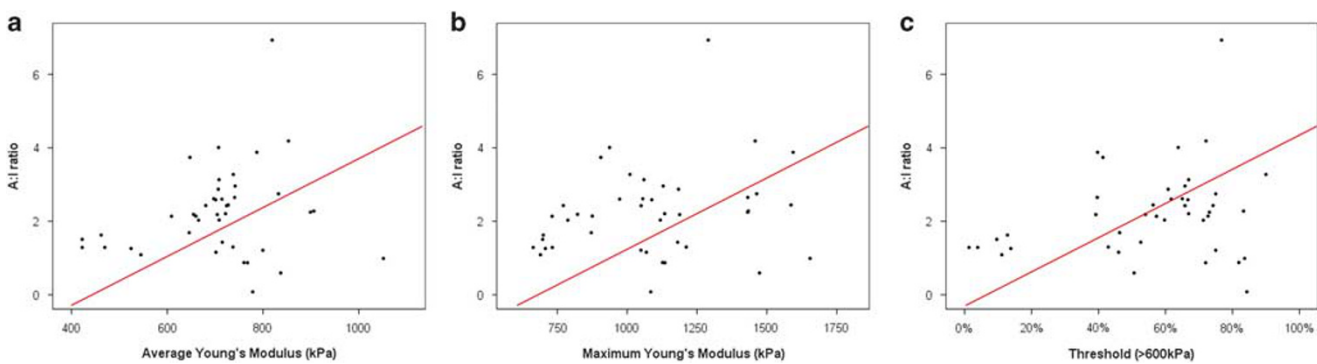
Figure 7 Scatterplots of the correlation of Young's modulus and collagen orientation (A:I ratio) using the (**a**) average method, (**b**) maximum method, and (**c**) threshold method.

Table 1 Disparity of Gleason score between initial TRUS biopsy and final prostatectomy

Patient number	Biopsy stiffness (kPa)[a]	A:I ratio	Gleason grade of biopsies	Gleason grade of radical prostatectomy	
1	631.07		3+3	3+4	7
2	795.16	1.79	3+3, 3+4	3+4	7
3	649.02	1.29	3+3	3+4	7
4	809.61	2.55	4+3, 4+4, 4+5, 5+4	4+5	9
5	707.69		3+3, 3+4, 4+3	3+4	7
6	900.99		3+5, 4+4, 4+5	4+5	9
7	658.93		3+3	3+4	7
8	728.25		3+3, 3+4	3+4	7
9	739.24		3+3, 4+3	4+3	7

[a]Biopsy stiffness (kPa) is the weighted mean of the stiffest biopsy among 12 biopsies.

As depicted in Figure 7, the biopsies with a Young's modulus lower than 800 kPa have a smaller A:I ratio.

Prediction of Histological Grade of Radical Prostatectomy

Eleven men underwent laparoscopic radical prostatectomy surgery, but two of them received a second biopsy before prostatectomy and were excluded from our study. Three patients (patients no.1, 3, and 7) had an upgrading in disease from a low to high Gleason score following radical prostatectomy (Table 1). Table 1 summarizes biopsy stiffness, A:I ratio, initial Gleason grade, and final Gleason grade of radical prostatectomy. It is noteworthy that biopsy stiffness (kPa) is the weighted mean of the stiffest biopsy amongst 12

biopsies. The ROC curve of the analysis method using average Young's modulus has the highest AUC (93.9%). According to the analysis of variance (ANOVA) analysis of the average method, the upper bound for Gleason 6 is 626.41 kPa at a 95% confidence interval for mean. Hereby, these three patients should be stratified to a higher Gleason score.

DISCUSSION
In this study, we demonstrated an optical characterization of the microstructural details of prostate tissue obtained from a large number of TRUS-guided biopsies using high-resolution OCE and SHG imaging. The method appeared to be highly accurate in differentiating cancer from normal benign prostatic tissue. It also provided accurate characterization of the Gleason grade based on the measurement of Young's modulus (tissue stiffness) and orientation of collagen around malignant lesions. OCT provides ultrastructural details of the tissues, and elastograms offer additional details and clarity. The technique could predict a higher Gleason grade disease with the final histopathological examination of a radical prostatectomy specimen. It may help in bridging the disparity between histopathological Gleason grades of a TRUS biopsy and radical prostatectomy samples. Furthermore, the technique has real potential for being employed during surgery of the prostate to guide dissection between peripherally located cancer tissue and neurovascualar bundles. With future engineering and research aimed at *in vivo* stiffness measurement and peri-tumoral collagen orientation, a multiscale imaging of PCa through a needle can be possible. The ultimate goals, to be achieved through future research following this work, are *in situ* detection and characterization of PCa to permit a more precise focal treatment, and scanning of the surface of the excised prostate gland intraoperatively to provide the surgeon with an assessment of tumor margins within minutes of prostate removal. Several challenges must be addressed before a complete translational landscape is possible. Heterogeneity of tissues, including diathermied tissue on the surface of prostate, and presence of blood could have an effect on the penetration of light. However, an excised piece of tissue followed by washing with normal saline could be utilized within surgical theaters for margin status assessment.

As demonstrated in the structural images of prostate biopsies, clear differences were noticed between benign and malignant groups. Benign prostate biopsy tissues were observed to have irregular and hollow glandular lumens in 2D/3D images, whereas those that were malignant lacked a lumenal structure with an increment of light reflectivity. With further use of a different objective lens, the imaging resolution of OCT could be increased to 1–2 μm, which will uncover more structural details of a prostate biopsy, and enhance the capacity of optical biopsy. The functional OCE, used in this study measured vibrational amplitude (surrogate markers of mechanical properties) of the freshly obtained prostate specimens following mechanical loading of tissues. The tissue stiffness estimated from this parameter was then employed to categorize specimens into different histological classifications. Further quantitative 3D elastograms of a prostate biopsy were reconstructed in high resolution from consecutive 2D elastograms. Both structural images and elastograms obtained with the OCE system were compared with histopathology as a reference standard to evaluate the diagnostic accuracy of the technique. A high diagnostic accuracy (with AUC > 90%) of classification of normal and cancerous tissues was presented in an *ex vivo* setting according to quantitative OCE. In addition, point-to-point comparison between histological imagery and elastograms illustrated a high accuracy when studying the underlying microscale elastic properties. This indicates that OCE can be a promising imaging tool for PCa detection with high sensitivity and specificity for malignant prostate diseases. With the average method, the stiffness of cancer biopsies was ~ 57.63% higher than that of those that were benign with corresponding stiffness values of 698.43 ± 125.29 *vs* 443.07 ± 88.95 kPa.

The gold standard histopathological analysis requires the expertise of a trained histopathologist. An inter-observer variation exists between two histopathologists besides the difficulties in characterizing lesions smaller than 3 mm. Microstructure, which may be missed by unaided eyes could explain the cases in this study where several areas of benign tissue had a higher stiffness than most. It was noted that the Young's modulus determined herein was higher than the literature.[15,33] The prostate biopsy samples in this study were fixed in formalin before the OCE experiment, which ensured the subsequent histopathological analysis of the cellular structure of the fixed biopsy was conducted smoothly. Formalin is predominantly used to fix tissue by cross-linking the proteins and hindering the biological degradation process. It increases tissue stiffness which, to some extent, can bias the final elasticity of prostate biopsies. In our experiment, the timeline was precisely controlled to finish every experiment. As all samples were fully fixed[30] in formalin for 24 h, the extent of stiffness increase should have been the same for all the benign and malignant prostate tissues.

Within the tissue stroma, collagen is the main structural and mechanical component. Changes in collagen alignment have been reported in the stroma of breast cancer tissue when compared with normal breast tissue.[34,35] In our study, the prostate biopsy was scanned via multiphoton microscopy with the SHG signal collected in the forward direction. The collagen pattern was then generated for each biopsy, and the orientation of collagen fibers was computed by FFT-SHG. The results from the SHG images were found to be correlated with the histological reports. The benign biopsy had a papillary collagen pattern, whereas the malignant biopsy had a reticular collagen pattern. Isotropic collagen fibers were seen in the benign prostate tissue without a preferred orientation. However, the collagen distribution in the malignant biopsies tended to be more oriented to the

same direction as the cancer became more aggressive. The correlation between collagen orientation and Gleason score, as well as the relationship between the orientation and tissue stiffness was analyzed in this study. The collagen orientation details addressed the tissue stiffness increase in the malignant prostate compared with the benign version. In a small group of men undergoing radical prostatectomy, the Young's modulus and collagen orientation were used to predict the final Gleason histopathological score (Table 1). This certainly necessitates further work to assess any potential use of these techniques in risk stratifying men with PCa.

In conclusion, the imaging of the mechanical properties of prostate tissue using OCE and the orientation analysis of peri-tumoral collagen by SHG imaging presented the possibility of optical modalities for the identification and characterization of PCa. The results from this study form the basis for future research employing these techniques for *in vivo* assessment of PCa and intraoperative assessment of tumor margins. The study is a first attempt at this scale to perform a detailed analysis of the microstructural details of human PCa tissue using elastograms and orientation of collagen around cancerous lesions. The biopsy stiffness and collagen orientation together constitute the new biomechanical markers of PCa with a very high diagnostic accuracy in terms of Gleason grade of cancerous tissues.

DISCLOSURE/CONFLICT OF INTEREST
The authors declare no conflict of interest.

1. Arora R, Koch MO, Eble JN, *et al.* Heterogeneity of Gleason grade in multifocal adenocarcinoma of the prostate. Cancer 2004;100: 2362–2366.
2. Humphrey PA. Gleason grading and prognostic factors in carcinoma of the prostate. Mod Pathol 2004;17:292–306.
3. Cohen MS, Hanley RS, Kurteva T, *et al.* Comparing the Gleason prostate biopsy and Gleason prostatectomy grading system: the Lahey Clinic Medical Center experience and an international meta-analysis. Eur Urol 2008;54:371–381.
4. Serefoglu EC, Altinova S, Ugras NS, *et al.* How reliable is 12-core prostate biopsy procedure in the detection of prostate cancer? Can Urol Assoc J 2013;7:E293–E298.
5. Chien GW, Slezak JM, Harrison TN *et al.* Health-related quality of life outcomes from a contemporary prostate cancer registry in a large diverse population. BJU Int 2017;120:520–529.
6. Waljee JF, Hu ES, Newman LA, *et al.* Predictors of re-excision among women undergoing breast-conserving surgery for cancer. Ann Surg Oncol 2008;15:1297–1303.
7. Cabioglu N, Hunt KK, Sahin AA, *et al.* Role for intraoperative margin assessment in patients undergoing breast-conserving surgery. Ann Surg Oncol 2007;14:1458–1471.
8. Nunez LV, Buttaro MA, Morandi A, *et al.* Frozen sections of samples taken intraoperatively for diagnosis of infection in revision hip surgery. Acta Orthop 2007;78:226–230.
9. Nguyen FT, Zysk AM, Chaney EJ, *et al.* Intraoperative evaluation of breast tumor margins with optical coherence tomography. Cancer Res 2009;69:8790–8796.
10. Haka AS, Volynskaya Z, Gardecki JA, *et al. In vivo* margin assessment during partial mastectomy breast surgery using raman spectroscopy. Cancer Res 2006;66:3317–3322.
11. Krouskop TA, Wheeler TM, Kallel F, *et al.* Elastic moduli of breast and prostate tissues under compression. Ultrason Imaging 1998;20: 260–274.
12. Zaman MH, Trapani LM, Sieminski AL, *et al.* Migration of tumor cells in 3D matrices is governed by matrix stiffness along with cell-matrix adhesion and proteolysis. Proc Natl Acad Sci USA 2006;103: 10889–10894.
13. Tang J, Zhang Y, Zhang MB, *et al.* Tissue elasticity displayed by elastography and its correlation with the characteristics of collagen type I and type III in prostatic stroma. Asian J Androl 2014;16:305–308.
14. Hoyt K, Castaneda B, Zhang M, *et al.* Tissue elasticity properties as biomarkers for prostate cancer. Cancer Biomark 2008;4:213–225.
15. Ahmad S, Cao R, Varghese T, *et al.* Transrectal quantitative shear wave elastography in the detection and characterisation of prostate cancer. Surg Endosc 2013;27:3280–3287.
16. Woo S, Kim SY, Cho JY, *et al.* Shear wave elastography for detection of prostate cancer: a preliminary study. Korean J Radiol 2014;15:346–355.
17. Li C, Guan G, Ling Y, *et al.* Detection and characterisation of biopsy tissue using quantitative optical coherence elastography (OCE) in men with suspected prostate cancer. Cancer Lett 2015;357:121–128.
18. Varghese T. Quasi-static ultrasound elastography. Ultrasound Clin 2009;4:323–338.
19. Kennedy BF, Kennedy KM, Sampson DD. A review of optical coherence elastography: fundamentals, techniques and prospects. IEEE J Select Topics Quant Electron 2014;20:272–288.
20. Kennedy KM, Ford C, Kennedy BF, *et al.* Analysis of mechanical contrast in optical coherence elastography. J Biomed Opt 2013;18:121508.
21. Kennedy KM, Kennedy BF, McLaughlin RA, *et al.* Needle optical coherence elastography for tissue boundary detection. Opt Lett 2012;37:2310–2312.
22. Chau AH, Chan RC, Shishkov M, *et al.* Mechanical analysis of atherosclerotic plaques based on optical coherence tomography. Ann Biomed Eng 2004;32:1494–1503.
23. Tuxhorn JA, Ayala GE, Rowley DR. Reactive stroma in prostate cancer progression. J Urol 2001;166:2472–2483.
24. Campagnola P. Second harmonic generation imaging microscopy: applications to diseases diagnostics. Anal Chem 2011;83:3224–3231.
25. Rao RAR, Mehta MR, Toussaint KC. Fourier transform-second-harmonic generation imaging of biological tissues. Optics Express 2009;17: 14534–14542.
26. Matteini P, Ratto F, Rossi F, *et al.* Photothermally-induced disordered patterns of corneal collagen revealed by SHG imaging. Opt Express 2009;17:4868–4878.
27. Cicchi R, Kapsokalyvas D, Troiano M, *et al. In vivo* non-invasive monitoring of collagen remodelling by two-photon microscopy after micro-ablative fractional laser resurfacing. J Biophotonics 2014;7: 914–925.
28. Ling Y, Li C, Feng K, *et al.* Second harmonic generation (SHG) imaging of cancer heterogeneity in ultrasound guided biopsies of prostate in men suspected with prostate cancer. J Biophotonics 2017;10:911–918.
29. Sheikh N, Wei C, Szewczyk-Bieda M, *et al.* Combined T2 and diffusion-weighted MR imaging with template prostate biopsies in men suspected with prostate cancer but negative transrectal ultrasound-guided biopsies. World J Urol 2017;35:213–220.
30. Ling Y, Li C, Feng K, *et al.* Effects of fixation and preservation on tissue elastic properties measured by quantitative optical coherence elastography (OCE). J Biomech 2016;49:1009–1015.
31. Li C, Guan G, Reif R, *et al.* Determining elastic properties of skin by measuring surface waves from an impulse mechanical stimulus using phase-sensitive optical coherence tomography. J R Soc Interface 2012;9:831–841.

32. Guan G, Li C, Ling Y, *et al.* Quantitative evaluation of degenerated tendon model using combined optical coherence elastography and acoustic radiation force method. J Biomed Opt 2013;18:111417.

33. Barr RG, Memo R, Schaub CR. Shear wave ultrasound elastography of the prostate: initial results. Ultrasound Q 2012;28:13–20.

34. Conklin MW, Eickhoff JC, Riching KM, *et al.* Aligned collagen is a prognostic signature for survival in human breast carcinoma. Am J Pathol 2011;178:1221–1232.

35. Provenzano P, Eliceiri K, Campbell J, *et al.* Collagen reorganization at the tumor-stromal interface facilitates local invasion. BMC Med 2006;4:1–15.